Comput Mech (2013) 51:961–974
DOI 10.1007/s00466-012-0778-7

ORIGINAL PAPER

A nonlocal continuum damage mechanics approach to simulation of creep fracture in ice sheets

Ravindra Duddu · Haim Waisman

Received: 26 March 2012 / Accepted: 7 August 2012 / Published online: 30 August 2012

Abstract We present a Lagrangian finite element formulation aimed at modeling creep fracture in ice-sheets using nonlocal continuum damage mechanics. The proposed formulation is based on a thermo-viscoelastic constitutive model and a creep damage model for polycrystalline ice with different behavior in tension and compression. In this paper, mainly, we detail the nonlocal numerical implementation of the constitutive damage model into commercial finite element codes (e.g. Abaqus), wherein a procedure to handle the abrupt failure (rupture) of ice under tension is proposed. Then, we present numerical examples of creep fracture under four-point bending, uniaxial tension, and biaxial tension in order to illustrate the viability of the current approach. Finally, we present simulations of creep crack propagation in idealized rectangular ice slabs so as to estimate calving rates at low deformation rates. The examples presented demonstrate the mesh size and mesh directionality independence of the proposed nonlocal implementation.

Keywords Ice mechanics · Creep fracture · Anisotropic damage · Finite element simulation · Nonlocal integral

R. Duddu (✉) · H. Waisman
Department of Civil Engineering and Engineering Mechanics, Columbia University, 610 Seeley W. Mudd Building, 500 West 120th Street, Mail Code 4709, New York, NY 10027, USA
e-mail: rduddu@gmail.com; ravidra.duddu@vanderbilt.edu

Present Address:
R. Duddu
Department of Civil and Environmental Engineering, Vanderbilt University, 400 24th Avenue South, 274 Jacobs Hall, Nashville, TN 37212, USA

1 Introduction

Creep fracture plays an important role in the calving of icebergs from glaciers and in the catastrophic collapse of ice-shelfs [1]. A better understanding of creep fracture mechanics is required to estimate the loss of mass from polar ice-sheets and to predict the consequent sea-level change. Field observations indicate that the calving process involves initiation and propagation of large fractures or rifts in ice-sheets and ice-shelfs [2]. Current theoretical models for estimating calving rates and rift propagation rates are based on linear elastic fracture analysis and so they do not consider the effects of viscoelastic creep deformation [3–7]. Computational models can help us gain new insights into the processes leading to glacial calving and ice-sheet fracture, however, the numerical aspects of viscoelastic creep fracture simulation need to be addressed. Therefore, in this paper, we present a finite element formulation for modeling creep fracture based on nonlocal continuum damage theory that is applicable at low deformation rates encountered in glaciers.

The material response of polycrystalline ice that constitutes glaciers is highly nonlinear, viscoelastic, and anisotropic [8]. This nonlinear behavior of ice is due to the nucleation and progressive accumulation of distributed flat and planar micro-cracks. Therefore, in the case of ice it is sufficient to consider only damage [9], unlike metals where both damage due to micro-defects and plasticity due to dislocations needs to be considered [10]. Since it is difficult to account for the micro-cracks individually, continuum damage theory [11] is used to describe the creep damage and eventual rupture of ice [12–14]. Herein, we employ a creep damage model for ice, based on the Murakami model [15, 16], that captures the temperature and stress-state dependent mechanical response of ice [17]. In addition, the anisotropy

arising from the micro-crack damage can be described using an anisotropy parameter.

Generally, creep damage in materials is distributed over a characteristic volume or characteristic length scale [18,19]. Physically, when distributed damage at the micro-scale reaches a critical level one large macro-crack may form leading to the failure of the characteristic volume of material. Previously, the topic of creep damage in polycrystalline materials such as light alloys, high-strength steels, copper etc., has been extensively studied using local creep damage models that do not consider any material length scale or damage localization (see [20] for a comprehensive literature review). Moreover, the finite element implementation of local creep damage [16] results in pathological mesh dependence, therefore, unreliable and also thermodynamically inconsistent [21]. By introducing a characteristic length scale through a nonlocal integral formulation [22,23] the nonlocal behavior can be captured and the pathological mesh dependence can be alleviated leading to consistent numerical results. Another approach is to use an explicit/implicit nonlocal gradient formulation [24] and the implicit gradient formulation is found to be largely equivalent to the integral formulation [25,26]. A comprehensive literature review on the various nonlocal integral and gradient formulations is beyond the scope of this paper and the interested reader is referred to [27] for a detailed review.

For most numerical studies, the motivation for creep damage modeling arises from the need to estimate the creep life of structural components, which is essential to structural design and safety. The finite element method therefore has been a popular choice for modeling creep damage evolution in structural components, especially, around blunt notches, sharp cracks, holes and connections [28–30]. However, previous investigations did not address, adequately, an important numerical issue of directional mesh bias of creep damage simulations associated with the finite element method; and so, it is considered in detail in the current work. Note that this problem of directional mesh bias arises particularly in the case of curved crack propagation under mixed-mode creep fracture and does not arise in the case of pure mode-I creep fracture [21]. Recently, the issue of directional mesh bias of brittle fracture simulations in concrete within the finite element framework has been investigated in [31,32]. Alternatively, mesh-free methods for damage, fracture, and localization problems may be pursued [33,34], although, the corresponding integration procedures may introduce some directional bias into the simulation results.

In this paper, we present a nonlocal integral formulation for creep damage that alleviates the problems of directional mesh bias and mesh size sensitivity associated with finite element analysis adequately. In addition, we propose strategies for numerical control of rupture in order to capture complete structural failure. An outline of the paper is as follows: Sect. 2 details the creep damage model equations and lists the values of the model parameters; Sect. 3 discusses the Lagrangian finite element framework, the solution strategy, the computational algorithm and procedure for rupture control; Sect. 4 presents numerical results for an ice beam under bending, for an ice plate under uniaxial and biaxial tension, and for a rectangular slab of ice under tension. Also, the results from local and nonlocal computations are compared. Finally, Sect. 5 gives some concluding remarks.

2 Constitutive damage model for polycrystalline ice

In this section, we briefly present a three dimensional viscoelastic damage model for polycrystalline ice that is valid for low stresses or low deformation rates. For more details the interested reader may refer [17]. The model equations for ice are presented using Einstein's notation (or the indicial notation), for clarity, and the standard summation convention is used for repeated indices. For example, the second-order stress tensor and strain tensor in indicial notation are given by,

$$\boldsymbol{\sigma} = \sigma_{ij}\, \boldsymbol{e}_i \otimes \boldsymbol{e}_j, \quad \boldsymbol{\epsilon} = \epsilon_{ij}\, \boldsymbol{e}_i \otimes \boldsymbol{e}_j, \tag{1}$$

where $\boldsymbol{e}_i$ denotes the orthonormal basis vectors of the Cartesian coordinate system, $\otimes$ denotes the dyadic product of vectors, and $i, j = \{1, 2, 3\}$ in three dimensions.

2.1 Notion of continuum damage

We consider an orthotropic continuum damage model based on the effective stress concept and the hypothesis of strain equivalence. We define a linear transformation (see Fig. 1) [35],

$$\tilde{\sigma}_{ij} = M_{ijkl}\sigma_{kl}, \tag{2}$$

where σ_{ij} is the Cauchy stress tensor representing the force per unit damaged area (including voids or cracks) in the physical space, $\tilde{\sigma}_{ij}$ is the effective stress representing the force per unit undamaged area (not including voids or cracks) in the effective space, and M_{ijkl} is the fourth-order damage effect tensor that characterizes the state of damage. The relation between the damage effect tensor, M_{ijkl} and the damage tensor, D_{ij}, is, [36,37],

$$M_{ijkl} = \frac{1}{2}(\omega_{ik}\delta_{jl} + \omega_{jk}\delta_{il}), \tag{3}$$

where ω_{ij} can be expressed in the indicial notation as,

$$\omega_{ik}(\delta_{kj} - D_{kj}) = \delta_{ij}, \tag{4}$$

or, in the matrix notation as,

$$\boldsymbol{\omega} = (\mathbf{1} - \boldsymbol{D})^{-1}. \tag{5}$$

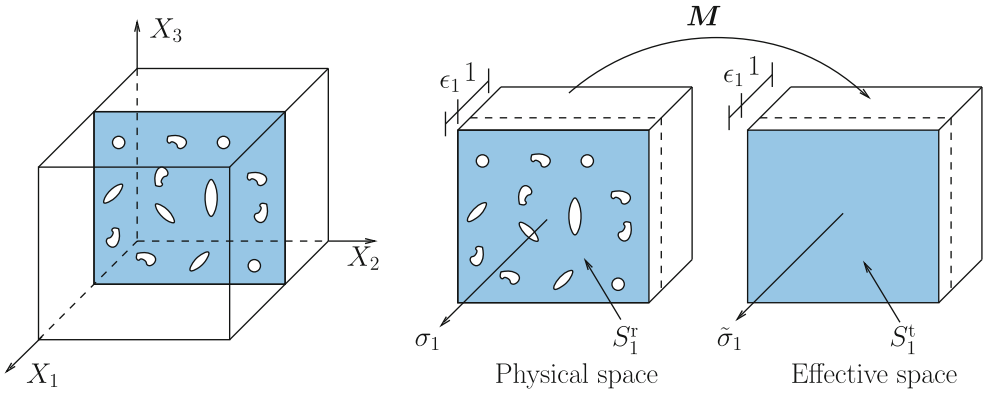

Fig. 1 Schematic illustration of the physical and effective spaces and the hypothesis of strain equivalence. The total or reference cross-sectional area is S_1^{t} and the area of micro-voids and micro-cracks is S_1^{v}. Therefore, the reduced cross-sectional area excluding the area of micro-cracks and micro-voids is given by $S_1^{\mathrm{r}} = S_1^{\mathrm{t}} - S_1^{\mathrm{v}}$

In the above equation, $\mathbf{1}$ denotes the second order identity matrix and a "-1" in the superscript denotes the inverse operator. When the damage tensor $\boldsymbol{D}$ is resolved in its principal directions we get,

$$\boldsymbol{\omega} = \begin{bmatrix} 1-D_1 & 0 & 0 \\ 0 & 1-D_2 & 0 \\ 0 & 0 & 1-D_3 \end{bmatrix}^{-1} = \begin{bmatrix} \dfrac{1}{1-D_1} & 0 & 0 \\ 0 & \dfrac{1}{1-D_2} & 0 \\ 0 & 0 & \dfrac{1}{1-D_3} \end{bmatrix}, \tag{6}$$

where D_1, D_2 and D_3 are the principal values of $\boldsymbol{D}$. In the special case of isotropic damage one scalar variable is sufficient to describe the deteriorated state of the material since $D_1 = D_2 = D_3$ [11]. Now, physically the principal damage component D_1 represents the ratio of the area of micro-voids and micro-cracks, S_1^{v}, to the reference cross-sectional area, S_1^{t}, of the principal plane with the normal along the X_1 direction as shown in Fig. 1, that is,

$$D_1 = \frac{S_1^{\mathrm{v}}}{S_1^{\mathrm{t}}} \quad \Rightarrow \quad 1 - D_1 = \frac{S_1^{\mathrm{t}} - S_1^{\mathrm{v}}}{S_1^{\mathrm{t}}} = \frac{S_1^{\mathrm{r}}}{S_1^{\mathrm{t}}}, \tag{7}$$

where S_1^{r} denotes the reduced cross-sectional area due to micro-cracks and micro-voids. Then, we have,

$$\omega_1 = \frac{1}{1-D_1} = \frac{S_1^{\mathrm{t}}}{S_1^{\mathrm{r}}}, \tag{8}$$

Thus, the principal values ω_i, $i = \{1, 2, 3\}$ can be physically interpreted as the ratios of the reference cross-sectional areas S_i^{t} to the reduced cross-sectional areas S_i^{r}. It is important note that this physical or geometrical representation is valid only for isotropic and orthotropic damage [38].

Next, the hypothesis of strain equivalence assumes that [39], "the strain associated with a damaged state under the applied stress is equivalent to the strain associated with its undamaged state under the effective stress." Accordingly, the Hooke's laws in the physical and effective spaces are,

$$\begin{cases} \tilde{\sigma}_{ij} = C^{\mathrm{e}}_{ijkl}\epsilon^{\mathrm{e}}_{kl}, \\ \sigma_{ij} = C^{\mathrm{dam}}_{ijkl}\epsilon^{\mathrm{e}}_{kl}, \end{cases} \tag{9}$$

where C^{e}_{ijkl} is the undamaged elasticity tensor and C^{dam}_{ijkl} is the elasticity tensor including the effect of damage. From Eqs. (2) and (9), we can see that,

$$C^{\mathrm{dam}}_{ijkl} = [M^{-1}]_{ijmn} C^{\mathrm{e}}_{mnkl}. \tag{10}$$

where "-1" in the superscript denotes the inverse operator.

Remark 1 Since we assume isotropic behavior of undamaged polycrystalline ice, C^{e}_{ijkl} can be written in terms of the Young's modulus, E, and Poisson's ratio, ν of ice. The Young's modulus of ice, generally derived from acoustic velocity measurements on ice specimens, depends on its density [4] and so it varies for each sample.

2.2 Constitutive equations for damaged ice

Herein, we briefly present the viscoelastic constitutive model for polycrystalline ice. Assuming small strains, the additive decomposition of the total strain tensor into its components is assumed as,

$$\epsilon_{ij} = \epsilon^{\mathrm{e}}_{ij} + \epsilon^{\mathrm{d}}_{ij} + \epsilon^{\mathrm{v}}_{ij}, \tag{11}$$

where the superscripts e, d, and v denote the elastic (time-independent and recoverable component), delayed elastic (time-dependent and recoverable component) and viscous (time-dependent and irrecoverable component) components, respectively.

Remark 2 Typically, creep behavior in polycrystalline materials at high temperatures (or temperatures close to the material's melting point) is classified into three distinct phases: primary, secondary, and tertiary [40]. In the current model, the behavior in the primary and secondary phases is described by the delayed elastic and viscoelastic models, respectively, and the behavior in the tertiary phase is captured by the creep damage model. The contribution of the delayed elastic component in the tertiary phase of creep can be neglected.

The relation for the viscous strain component is given by a power law rate equation as,

$$\dot{\epsilon}^{\mathrm{v}}_{ij} = \frac{3}{2} K_N \left(\frac{3}{2} \tilde{\sigma}^{\mathrm{dev}}_{kl} \tilde{\sigma}^{\mathrm{dev}}_{kl} \right)^{(N-1)/2} \tilde{\sigma}^{\mathrm{dev}}_{ij}, \tag{12}$$

where K_N is the viscosity coefficient, N is the viscous exponent, the effective deviatoric stress is given by,

$$\tilde{\sigma}^{\mathrm{dev}}_{ij} = \tilde{\sigma}_{ij} - \frac{1}{3} \tilde{\sigma}_{kk} \delta_{ij}, \tag{13}$$

and δ_{ij} denotes the Kronecker's delta.

Remark 3 Equation12 is a multiaxial generalization of the well known Glen's law in ice mechanics [41] and the viscosity coefficient K_N is reported to be temperature dependent. Also, the viscous strains depend only the deviatoric part of the effective stress and so there is no volume change associated with the viscous deformation.

The delayed elastic strain is given by a rate equation as,

$$\dot{\epsilon}^{d}_{ij} = A \left(\frac{3}{2} K \tilde{\sigma}^{\mathrm{dev}}_{ij} - \epsilon^{d}_{ij} \right), \tag{14}$$

where A and K are material parameters. Thus, the delayed elastic and viscous strains are given by first order differential equations in time.

2.3 Damage evolution

The damage evolution law describes the growth of damage that leads to eventual failure of the material. This anisotropic creep damage law [17] captures: (i) multi-axial behavior; (ii) different failure behavior in tension, compression and shear; (iii) temperature dependence; and (iv) damage induced directional anisotropy. In a Lagrangian framework, the damage evolution rate is given by,

$$\dot{D}_{ij} = \begin{cases} f_{ij}, & \text{if } \max\{\epsilon_{ij}\} \geq \epsilon_{th}, \\ 0, & \text{if } \max\{\epsilon_{ij}\} < \epsilon_{th}, \end{cases} \tag{15}$$

where f_{ij} is the damage evolution function and ϵ_{th} is a strain threshold for damage initiation. The generalized form of f_{ij} is given by,

$$f_{ij} = B \, \langle \chi \rangle^{r} \, (\omega_{kl} \xi^{(1)}_{k} \xi^{(1)}_{l})^{k_\sigma} \left[(1-\gamma)\delta_{ij} + \gamma \xi^{(1)}_{i} \xi^{(1)}_{j} \right], \tag{16}$$

$$\chi = \alpha \tilde{\sigma}^{(1)} + \beta \sqrt{\frac{3}{2} \tilde{\sigma}^{\mathrm{dev}}_{mn} \tilde{\sigma}^{\mathrm{dev}}_{mn}} + (1 - \alpha - \beta) \tilde{\sigma}_{kk}, \tag{17}$$

where B, r, k_σ, γ are model parameters, $\tilde{\sigma}^{(1)}$ is the maximum eigenvalue of the effective stress tensor, $\tilde{\sigma}_{ij}$; $\boldsymbol{\xi}$ is the eigenvector associated with $\tilde{\sigma}^{(1)}$; χ is the Hayhurst's equivalent stress measure and a function of the effective stress tensor, $\tilde{\sigma}$; α, β are the materials parameters that describe the brittle-ductile failure behavior; and the Macaulay brackets are defined as $\langle \chi \rangle = \dfrac{\chi + |\chi|}{2}$.

Remark 4 In Eq. (17) the parameter B is temperature dependent and the tensor ω_{ij} is function of the damage tensor D_{ij}. Consequently, $\boldsymbol{f}$ is function of the Cauchy stress tensor, $\boldsymbol{\sigma}$, the temperature, T, and the damage tensor, $\boldsymbol{D}$.

Remark 5 Creep damage in ice is primarily due to formation of micro-cracks at fine scale that is modeled, herein, using a continuum damage mechanics approach. As damage evolves, micro-cracks nucleate and grow perpendicular to the principal tensile stresses. This leads to the reduction of material strength or stiffness only of the cross-sections with normals along the principal tensile stress directions and so it introduces directional anisotropy. This behavior is modeled using the anisotropy parameter, γ, as originally proposed by Murakami [15,16]. By definition, $0 \leq \gamma \leq 1$, with $\gamma = 0$ for pure isotropic damage evolution and $\gamma = 1$ for pure anisotropic damage evolution.

The presence of an existing micro-crack or micro-void leads to a stress concentration in its vicinity and so new damage (i.e. micro-crack or micro-void growth and nucleation) usually occurs near the existing defect. Thus, existing damage enhances the damage rate in tension, but it does not effect the damage rate in compression, since compression tends to temporarily close the existing cracks. However, in the case of compression dynamic recrystallization occurs during the tertiary phase of ice creep [42], decreasing the damage rate. This stress state dependent behavior or tension–compression asymmetry of ice is described by the parameter k_σ as,

$$k_\sigma = \begin{cases} [k_1 + k_2 |\sigma_{ii}|], & \text{if } 0 \leq \sigma_{ii} \leq 1 \text{ MPa (tension)}, \\ -[k_3 + k_4 |\sigma_{ii}|], & \text{if } -3 \text{ MPa} \leq \sigma_{ii} < 0 \text{ (compression)}, \end{cases} \tag{18}$$

where k_1, k_2, k_3, and k_4 are parameters determined using a linear fit.

2.4 Model parameters

A total of 13 model parameters describe the coupled viscoelastic damage model. The parameters, K_N, N, A, K, E, ν describe the viscoelastic constitutive behavior of ice; and the parameters, $\alpha, \beta, B, r, k_\sigma, \epsilon_{\mathrm{th}}$ and γ describe the anisotropic damage behavior of ice. The values of these parameters are generally determined using laboratory test data of ice

creep under uniaxial tension or compression. The deformation response of ice under shear is similar to that under compression [43]; however, due to the lack of experimental data under shear loading, we assume the parameter values calibrated under compression to hold under shear as well. The physical significance of each parameter, their temperature dependence and the procedure to calibrate them is detailed in [17]. Herein, we perform all the simulations at a constant temperature of $T = -10\,^{\circ}\mathrm{C}$ and the values of the parameters used are given in Table 1.

Remark 6 The temperature dependencies of the parameters K_N and B, given by Arrhenius (exponential) type relations, are calibrated using published experimental data of laboratory ice specimens [17]. These two parameters K_N and B increase with temperature, consequently, ice flows and damages at a faster rate at higher temperatures. Therefore, the ice specimen will fail early at higher temperatures, exhibiting lower material strength; however, the predicted crack paths under a specific multiaxial loading configuration would be similar at different temperatures.

3 Strain-based finite element formulation

3.1 Governing equations

We use a Lagrangian description of motion wherein the material coordinates are denoted by $\boldsymbol{X} = \{X_i \mathbf{e}_i, i = 1, 2, 3\}$. The displacement vector at a material point $\boldsymbol{X}$ at time t is given by $\boldsymbol{u}(\boldsymbol{X}, t) = \{u_i \mathbf{e}_i, i = 1, 2, 3\}$. The equilibrium equation together with the constitutive law, strain–displacement relations, and the boundary conditions defines the boundary value problem (BVP). For the sake of completeness the governing equations are briefly reviewed. The strong form of the BVP describing the viscoelastic deformation process is: find $\boldsymbol{u}(\boldsymbol{X}, t)\ \forall\, t \in [0, \tau]$ such that,

$$\begin{aligned} &\frac{\partial \sigma_{ij}}{\partial X_j} + \rho\, b_i = 0 \text{ in } \Omega, \\ &u_i = u_i^g \qquad \text{on } \Gamma^u, \\ &\Sigma_i = \sigma_{ij} n_j \qquad \text{on } \Gamma^t, \end{aligned} \tag{19}$$

where Ω is the problem domain, Γ^u and Γ^t denote the Dirichlet and Neumann parts of the boundary for the equilibrium equation, respectively; $\boldsymbol{\Sigma}$ is the traction vector on a surface with outward normal $\mathbf{n}$; and τ is the end time of the simulation. The boundary of the computational domain is partitioned such that $\Gamma^u \bigcap \Gamma^t = \emptyset$ and $\Gamma^u \bigcup \Gamma^t = \Gamma$. Initially, ice is assumed to be undamaged, that is, $\boldsymbol{D}(\boldsymbol{X}, 0) = 0$. The Cauchy stress is computed as,

$$\begin{aligned} \sigma_{ij} &= [M^{-1}]_{ijkl} C^{\mathrm{e}}_{klmn} \epsilon^{\mathrm{e}}_{mn} \\ &= [M^{-1}]_{ijkl} C^{\mathrm{e}}_{klmn} \left(\epsilon_{mn} - \epsilon^{\mathrm{d}}_{mn} - \epsilon^{\mathrm{v}}_{mn}\right), \end{aligned} \tag{20}$$

where C^{e}_{klmn} is the fourth-order undamaged isotropic elasticity tensor and ϵ_{mn} is the total strain, which for small strains is given by,

$$\epsilon_{ij} = \frac{1}{2}\left(\frac{\partial u_i}{\partial X_j} + \frac{\partial u_j}{\partial X_i}\right). \tag{21}$$

Remark 7 The matrix $\boldsymbol{M}^{-1}$ in Eq. (20) can be evaluated by direct inversion of $\boldsymbol{M}$ at each material point. Note that in Voigt notation, $\boldsymbol{M}$ is: a 6×6 matrix in 3D and a 3×3 matrix in 2D plane stress. For 2D isotropic damage, $\boldsymbol{M}$ is a diagonal matrix with $M_{11} = M_{22} = M_{33}$. For anisotropic damage, $\boldsymbol{M}$ in Voigt notation is a nonsymmetric matrix and so the option "unsymm" with user material needs to be used in Abaqus.

3.2 Nonlocal integral formulation

Herein, we employ a nonlocal integral for evaluating the damage variable in order to ameliorate the computational scheme by alleviating the numerical problems associated with the local formulation. We start by defining a nonlocal damage rate $\hat{\dot{D}}_{ij}$ at the p^{th} material point $\boldsymbol{X}^p$ in the computational domain as,

$$\hat{\dot{D}}_{ij}(\boldsymbol{X}^p) = \frac{\int_\Omega \Phi(\boldsymbol{X}^p - \boldsymbol{X})\, \dot{D}_{ij}(\boldsymbol{X})\, d\boldsymbol{X}}{\int_\Omega \Phi(\boldsymbol{X}^p - \boldsymbol{X})\, d\boldsymbol{X}}, \tag{22}$$

where Φ is an assumed weighting function given by [26,31],

$$\Phi(\boldsymbol{X}^p - \boldsymbol{X}) = \exp\left(-\kappa \frac{||\boldsymbol{X}^p - \boldsymbol{X}||^2}{l_c^2}\right). \tag{23}$$

In the above equation, l_c is the characteristic nonlocal length scale and κ is a positive constant. Essentially, the nonlocal weighting function, Φ, defines a bell shaped surface so that as one moves farther from the point $\boldsymbol{X}^p$ we have $\Phi \to 0$, as shown in Fig. 2a. The constant $\kappa = 2$, in the current study, affects the rate of decay of the the weight function in the computational domain Ω. Note that l_c should be sufficiently larger than the mesh size h so that for each Gauss point $\boldsymbol{X}^p$ there are enough neighbors within the window of influence bounded by a circle of radius l_c, as shown in Fig. 2b.

Remark 8 Physically, the motivation for a nonlocal formulation arises from experimental observations on quasi-brittle materials that exhibit damage localization over narrow regions with a characteristic length scale [44]. Numerically, the need for the nonlocal damage formulation stems from the problems of mesh size and mesh alignment sensitivities [32], and loss of ellipticity under quasi-static conditions [45], of local damage formulations.

The finite element implementation of the nonlocal integral involves a summation to evaluate the nonlocal damage increment, $\Delta \hat{\boldsymbol{D}}$, given by,

Table 1 Model parameters for ice at temperature $T = -10\,^{\circ}\mathrm{C}$ (source [17])

Parameter	Value in tension	Value in compression/shear	Units
E	9,500	9,500	MPa
ν	0.35	0.35	–
A	1.5×10^{-3}	1.5×10^{-3}	s^{-1}
K	1.2×10^{-3}	1.2×10^{-3}	MPa^{-1}
N	3.1	3.1	–
K_N	2.56×10^{-7}	1.71×10^{-7}	$\mathrm{MPa}^{-N}\ \mathrm{s}^{-1}$
B	5.23×10^{-7}	5.23×10^{-5}	$\mathrm{MPa}^{-r}\ \mathrm{s}^{-1}$
r	0.43	1.0	–
k_1	−2.63	–	–
k_2	7.24	–	MPa^{-1}
k_3	–	12.36	–
k_4	–	−3.83	MPa^{-1}
α	0.21	0.0	–
β	0.63	0.84	–
γ	0.9	0.0	
ϵ_{th}	0.008	0.008	–

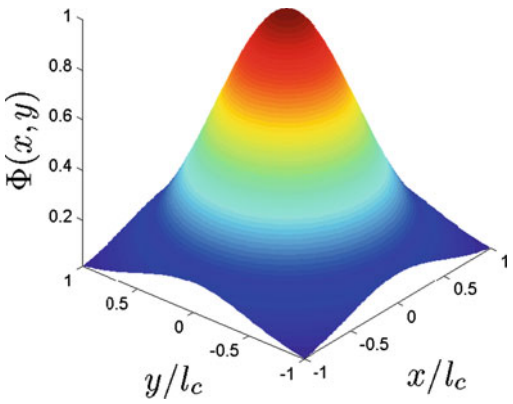

(a) Weight function $\Phi(\boldsymbol{X}^p - \boldsymbol{X})$ when $\boldsymbol{X}^p = (0,0)$ and $\boldsymbol{X} = (x, y)$

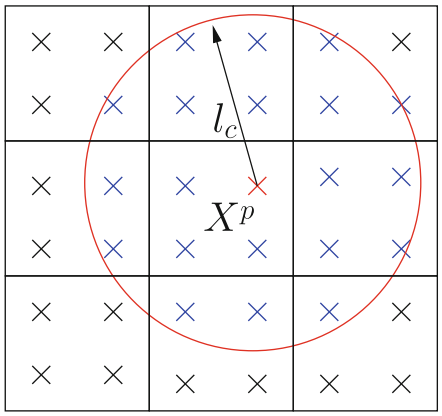

(b) Schematic diagram showing neighboring Gauss points of $\boldsymbol{X}^p$

Fig. 2 Nonlocal integral formulation and its finite element implementation in 2D. The Gauss point locations are indicated by ×s. The Gauss point $\boldsymbol{X}^p$ is colored in *red* and its neighbors are colored in *blue*. (Please refer to the online version for plots)

$$\Delta\hat{D}_{ij}(\boldsymbol{X}^p) = \frac{\sum_{l=1}^{N_{\mathrm{GP}}} \Phi(\boldsymbol{X}^p - \boldsymbol{X}^l)\, \Delta D_{ij}(\boldsymbol{X}^l)}{\sum_{l=1}^{N_{\mathrm{GP}}} \Phi(\boldsymbol{X}^p - \boldsymbol{X}^l)}, \tag{24}$$

$$\Phi(\boldsymbol{X}^p - \boldsymbol{X}^l) = \exp\left(-2\frac{||\boldsymbol{X}^p - \boldsymbol{X}^l||^2}{l_c^2}\right), \tag{25}$$

where N_{GP} is the number of neighboring Gauss points. Note that Eq. (24) is a weighted average that is an approximation of Eq. (22) using the midpoint method of numerical integration. In order to reduce the computational burden, at the first step of the computation, for each Gauss point we can identify and store the coordinates of its Gauss point neighbors within the window of influence as shown in Fig. 2b. Then, the weights for each neighbor and the sum of weights for each Gauss point can be computed and stored. For subsequent time steps one only needs to perform the summation given by Eq. (24) using the stored data.

3.3 Solution strategy

The creep damage model is implemented in Abaqus via the user defined subroutine UMAT [46]. The discretization of

the equilibrium equation in space using the finite element approximation is taken care of by Abaqus. Now, let us recall from Sect. 2.2 that the expressions for the viscous strain rate, delayed elastic strain rate, and damage rate given by ordinary differential equations in time. These rate equations are discretized in time using the explicit forward Euler method within our UMAT implementation. Most importantly, the updated stress and the consistent Jacobian (tangent stiffness) matrix need to be defined by the user. The detailed UMAT algorithm, using matrix notation, is described in the following Sect. 3.4.

Remark 9 Mainly, we assume that the viscoelastic damage process is quasi-stationary, that is, the ice specimen under the applied loading is at equilibrium during damage increments. The first time step of the numerical simulation is a purely elastic step, since damage is initialized to be zero, and the subsequent time steps capture creep and/or stress relaxation. The value of the Δt needs to be chosen so as to ensure convergence of the nonlinear iterative scheme used to solve the equilibrium equation.

As discussed in Sect. 2.4, the model parameters depend on the stress or stress-state. Therefore, at every time step t_n of the numerical simulation, one needs to calculate the viscous and damage parameters at each Gauss (integration) point. More specifically, to calculate the viscous parameters we check the sign of each effective stress component ${}^n\tilde{\sigma}_{ij}$ at time t_n: (i) if positive and $i = j$ then set viscous parameters values under pure tension; (ii) if negative and $i = j$ set viscous parameter values under pure compression; and (iii) if $i \neq j$ set viscous parameters values under pure shear. In order to calculate the damage parameters we check the sign of the first invariant of the effective stress tensor (i.e., sign of ${}^n\tilde{\sigma}_{ii}$) at time t_n: (i) if positive then set damage parameters values under pure tension; and (ii) if negative or zero then set damage parameters values under pure compression.

3.4 Detailed algorithm

The strain increment $\Delta\boldsymbol{\epsilon}$ is assumed by Abaqus solver and is a given quantity at time $t = t_n$. All the variables at time t_n, for example, the Cauchy stress, ${}^n\boldsymbol{\sigma}$, and the damage tensor, ${}^n\boldsymbol{D}$, are known. The computation essentially involves quantifying the variables at the next time step, that is, at time $t_{n+1} = t_n + \Delta t$. At each Gauss point, $\boldsymbol{X}^p$, $p = 1, 2..., N_{\mathrm{GP}}$:

1. Calculate ${}^n\boldsymbol{M}$ using Eq. (3) and then the effective stress as,

$$ {}^n\tilde{\boldsymbol{\sigma}} = {}^n\boldsymbol{M}\,{}^n\boldsymbol{\sigma}. \tag{26} $$

2. Depending on the sign of $\tilde{\sigma}_{ij}$ set the constitutive model parameters. Then, compute the increments of viscous and delayed elastic strain as,

$$ \Delta\boldsymbol{\epsilon}^{\mathrm{v}} = \frac{3}{2}K_N\Delta t\left(\frac{3}{2}\,{}^n\tilde{\sigma}^{\mathrm{dev}}_{kl}\,{}^n\tilde{\sigma}^{\mathrm{dev}}_{kl}\right)^{(N-1)/2}\,{}^n\tilde{\boldsymbol{\sigma}}^{\mathrm{dev}}, \tag{27} $$

$$ \Delta\boldsymbol{\epsilon}^{\mathrm{d}} = A\Delta t\left(\frac{3}{2}K\,{}^n\tilde{\boldsymbol{\sigma}}^{\mathrm{dev}} - {}^n\boldsymbol{\epsilon}^{\mathrm{d}}\right). \tag{28} $$

3. Compute the elastic strain increment as,

$$ \Delta\boldsymbol{\epsilon}^{\mathrm{e}} = \Delta\boldsymbol{\epsilon} - \Delta\boldsymbol{\epsilon}^{\mathrm{d}} - \Delta\boldsymbol{\epsilon}^{\mathrm{v}}. \tag{29} $$

4. Depending on the sign of $\tilde{\sigma}_{ii}$ set the damage model parameters. Then, calculate the local increment of damage as,

$$ \Delta\boldsymbol{D} = \begin{cases} \boldsymbol{f}\Delta t, & \text{if } \max\{\boldsymbol{\epsilon}\} \geq \epsilon_{\mathrm{th}}, \\ 0, & \text{if } \max\{\boldsymbol{\epsilon}\} < \epsilon_{\mathrm{th}}. \end{cases} \tag{30} $$

5. Compute the nonlocal increment of damage and update as,

$$ \Delta\hat{\boldsymbol{D}}(\boldsymbol{X}^p) = \frac{\sum_{l=1}^{N_{\mathrm{GP}}}\Phi(\boldsymbol{X}^p - \boldsymbol{X}^l)\,\Delta\boldsymbol{D}(\boldsymbol{X}^l)}{\sum_{l=1}^{N_{\mathrm{GP}}}\Phi(\boldsymbol{X}^p - \boldsymbol{X}^l)}, \tag{31} $$

$$ {}^{n+1}\boldsymbol{D} = {}^n\boldsymbol{D} + \Delta\hat{\boldsymbol{D}}. \tag{32} $$

6. Calculate the updated damaged elasticity matrix and its increment as,

$$ {}^{n+1}\boldsymbol{C}^{\mathrm{dam}} = \left[{}^{n+1}\boldsymbol{M}\right]^{-1}\boldsymbol{C}^{\mathrm{e}}. \tag{33} $$

7. Compute the increment of the Cauchy stress and update as,

$$ \Delta\boldsymbol{\sigma} = {}^{n+1}\boldsymbol{C}^{\mathrm{dam}}\,\Delta\boldsymbol{\epsilon}^{\mathrm{e}}, \tag{34} $$

$$ {}^{n+1}\boldsymbol{\sigma} = {}^n\boldsymbol{\sigma} + \Delta\boldsymbol{\sigma}. \tag{35} $$

8. Define the secant stiffness operator as,

$$ {}^{n+1}\boldsymbol{K} = \frac{\partial\Delta\boldsymbol{\sigma}}{\partial\Delta\boldsymbol{\epsilon}} = {}^{n+1}\boldsymbol{C}^{\mathrm{dam}}. \tag{36} $$

9. Update and store all solution dependent variables,

$$ {}^{n+1}\boldsymbol{\epsilon}^{\mathrm{d}} = {}^n\boldsymbol{\epsilon}^{\mathrm{d}} + \Delta\boldsymbol{\epsilon}^{\mathrm{d}}. \tag{37} $$

Remark 10 Even though damage evolution and viscous flow are formulated in stress-space, the above numerical implementation still leads to a strain-space formulation of the coupled viscoelastic damage problem because the stress tensor is a dependent function of the strain via the constitutive relations.

Note that Abaqus implements the UMAT algorithm one Gauss point at a time and lets the user only access the solution-dependent variables corresponding to that Gauss point. Therefore, in order to evaluate the nonlocal damage increment the user needs to define a common block to store the local damage increments, neighbors and the nonlocal weights for all Gauss points. However, this still does not help avoid a computational inconsistency since the weighting function is applied uniformly to all the damage values of different time steps. Basically, the nonlocal damage increment given by the weighted average in Eq. (31), takes into account the local damage increment values at all the neighbor Gauss points around the point $\boldsymbol{X}^p$, some of which are updated and the rest yet to be updated at a particular time interval. This leads to a semi-explicit formulation and in fact is a limitation of the proposed numerical implementation via the UMAT subroutine. One remedy is to use small time and strain increments, thereby, minimizing this inconsistency, which is employed herein. An alternative remedy, proposed by Chow et al. [47], is to subdivide the strain and time increments from the Abaqus main program into a certain number of sub-steps. Then, at each sub-step, calculate and update all the variables, but use only the variables computed at the final sub-step to form the tangent modulus for the Abaqus main program.

3.5 Numerical control of rupture

In this section we propose the following strategies in order to continue the computation up to complete structural failure:

1. *Secant operator*: We approximate the Jacobian matrix ${}^{n+1}\boldsymbol{K}$ with the secant stiffness matrix, as given by Eq. (36), for robustness; however, for better convergence with the risk of loss of robustness it is better to define a tangent operator [31]. Note that for nonlocal integral computations it is more difficult to derive a consistent tangent operator [48]. The derivation of the consistent tangent for the current nonlocal creep damage formulation is a topic of future research.
2. *Critical and maximum damage*: The damage in the tertiary phase of creep is marked by a sudden localized failure or "rupture", which presents a major problem for the numerical implementation. This numerical difficulty can be avoided by defining a critical damage D_{cr} and a maximum damage $D_{\max}$. For 2D isotropic damage, once the non-zero damage components $D_{11} = D_{22}$ reach D_{cr}, we can set the damage components $D_{11} = D_{22} = D_{\max}$ and the corresponding damage rates $\dot{\hat{D}}_{11} = \dot{\hat{D}}_{22} = 0$. We found that bounding the damage variable components by $D_{\text{cr}} = 0.6$ and $D_{\max} = 0.97$ helps continue the computation up to structural failure. For 2D anisotropic damage, $D_{11} \neq D_{22}$ and so it presents more complications, which is discussed in detail in [31].
3. *Damage rate control*: The current creep damage model defines a power law wherein the damage exponent k_σ is a function of the stress, as given by Eq. (18). The parameter k_σ has been calibrated for a particular stress range and so it is only valid for within that stress range [17]. However, near a notch or a crack the stress at a Gauss point can be quite large in a finite element computation owing to the stress singularity. Depending on the mesh size, the stresses near a notch can be outside the range of calibration resulting in a large value of k_σ. Herein, we cap the value of k_σ to be 30 to obtain consistent results. Further, we set an upper bound for the damage increment, $\Delta \boldsymbol{D}$, and the nonlocal damage rate, $\Delta \dot{\hat{\boldsymbol{D}}}$, equal to 0.05. This value is chosen in order to capture experimentally observed rupture behavior [17] as well as to obtain consistent nonlocal results with mesh refinement, as demonstrated in Sect. 4.2.

4 Numerical examples

4.1 Four point bending test

The purpose of this numerical investigation is to validate the computational model using experimental data of ice creep in bending. Experiments were conducted by Krausz [49] on ice beams that were simply supported at each end and loaded equally at their one-third points, as shown in Fig. 3a. Each load is 16.6 lbs producing a maximum bending moment of about 25 in.-lb per inch in the constant bending moment section of the beam. The ice beam is 4 inches wide and 1 inch thick with a span (distance between supports) of 18 inches. The experiments only reported the short term response of ice under bending for a total observation time of 10 h. In the current study, we considered only one experimental data set denoted as "Series 2" in [49].

To simulate this test we assume plane stress conditions. We take the ice material parameters from Table 1 and the density of ice to be 917 kg/m^3, the latter is needed to prescribe the body force due to gravity. The damage is assumed to be isotropic (i.e $\gamma = 0$) and the field output of the damage variable on the deformed mesh at $t = 150$ hours (h) is shown in Fig. 3a. The computed deflection–time relationship at the midpoint of the beam between $t = 0-10$ h is plotted along with the scatter of experimental data (Series 2) from [49] in Fig. 3b. This short term mechanical behavior, described by the delayed elastic and viscoelastic models, matches well with the experimental results. The computed long term behavior is shown in Fig. 3c, wherein, we can see that at around $t = 50$ h damage in ice accelerates leading to a complete structural failure at around $t = 170$ h.

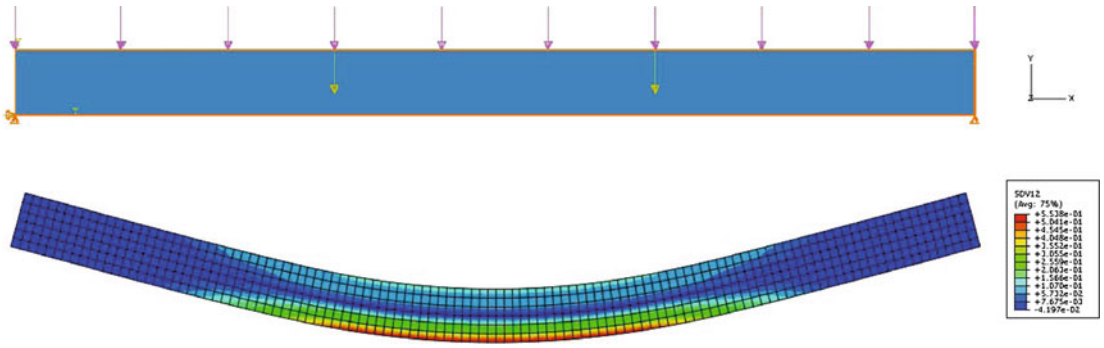

(a) Problem set up and field output of the damage variable

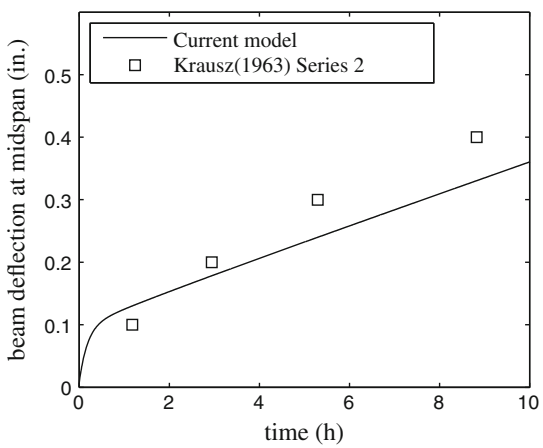

(b) Time evolution of the deflection at midspan for $t < 10$ h

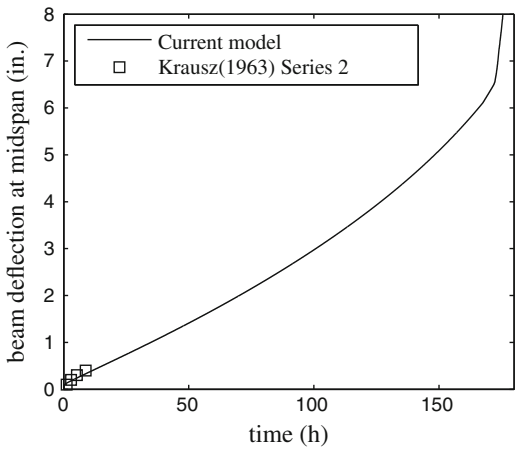

(c) Time evolution of deflection at midspan till complete structural failure at around $t = 170$ h

Fig. 3 Ice beam subjected to four point bending at $T = -10°$C. The maximum damage at $t = 150$ h is 0.55 at mid-span, as seen from the legend in sub-plot (**a**). In **b** and **c**, the experimental data of [49] is given by the scatter of squares; and the corresponding model fit is given by the *solid line*

4.2 Mode I creep crack growth

The objective of this study is to demonstrate the mesh size independence of the proposed nonlocal integral formulation for creep damage. Let us consider a rectangular slab of ice with a notch at the center of the top edge, as shown in Fig. 4. We assume plane stress conditions and apply a constant uniform strain rate at the right edge of the slab so as to propagate a mode I creep crack originating from the notch. The material parameters for ice are given in Table 1. Note that the isotropic model ($\gamma = 0$) and fully anisotropic model ($\gamma = 1$) yield the same damage evolution equation for $\dot{D}_{11}$ for uniaxial tension.

We consider four finite element meshes consisting of bilinear quadrilateral elements (CPS4 in Abaqus) with mesh sizes $h = 10, 5, 2.5, 1.25$ m. The numerical results of average pressure (p) versus applied strain (ϵ) at the right edge using a local damage formulation are given in Fig. 5a. We can see that upon mesh refinement the softening regime of the material model becomes steeper leading to a more abrupt failure. Furthermore, the area under the p versus ϵ curve is a measure of the energy dissipated during the damage process and the local damage model predicts different dissipation energies for different mesh sizes. This is because a local damage formulation suffers from pathological mesh dependence upon localization that constricts the damage zone width to one element size and so it is thermodynamically inconsistent

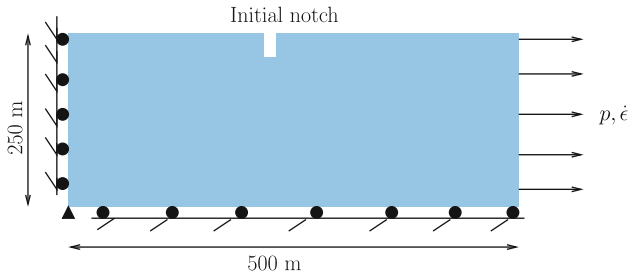

Fig. 4 Schematic representation of a notched rectangular ice slab loaded in uniaxial tension. A constant uniform strain rate of $\dot{\epsilon} = 1 \times 10^{-5}$ s^{-1} is applied at the right edge and the corresponding pressure p on that edge is calculated at several quasi-static time increments

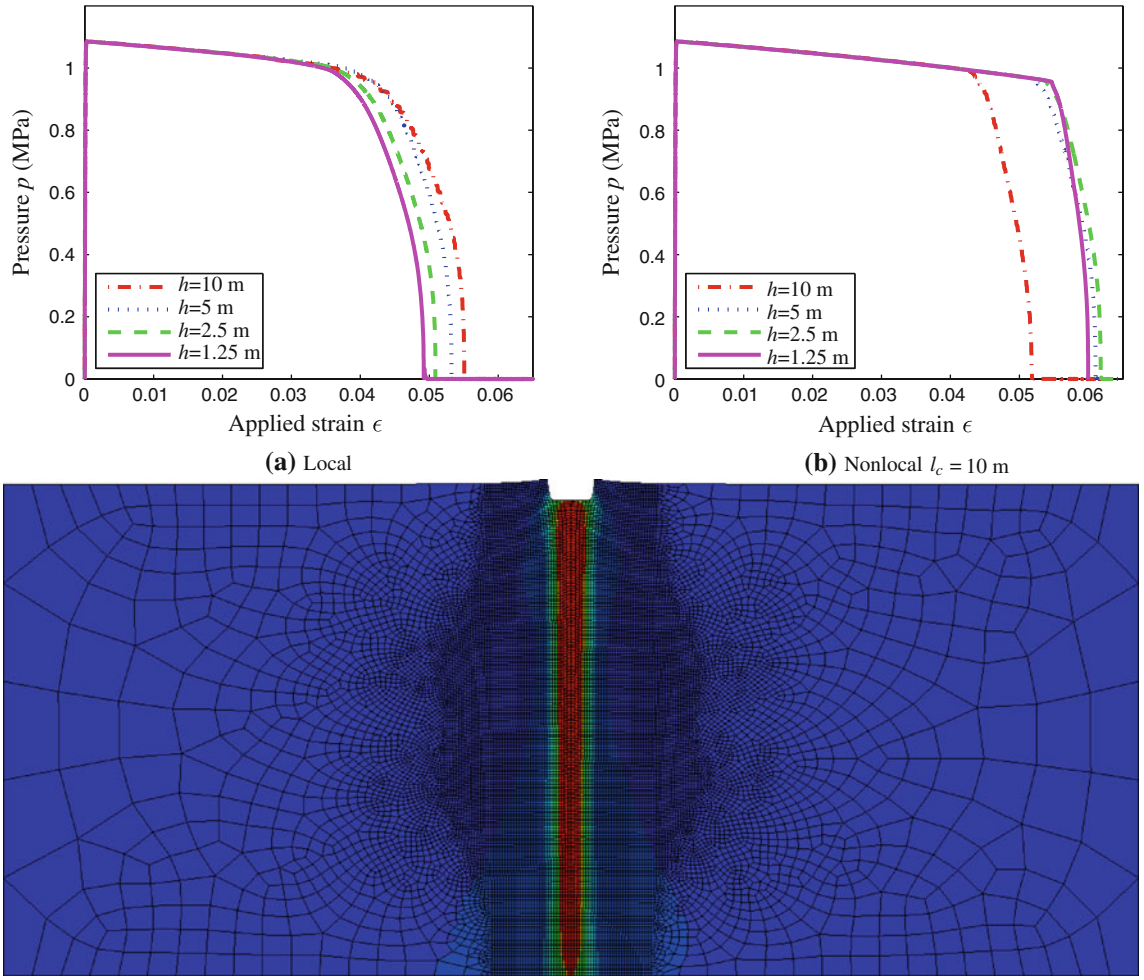

(a) Local

(b) Nonlocal $l_c = 10$ m

(c) Damage contour plot, $h = 1.25$ m and $l_c = 10$ m

Fig. 5 Mesh size sensitivity study for the local and nonlocal damage formulations. The nonlocal damage formulation is mesh size independent, therefore, is consistent. In the damage contour plot the elements colored in *red* have ruptured. The maximum damage is controlled, $D_{\max} = 0.97$, which helps continue the simulation until complete structural failure. (Please refer to the online version for plots)

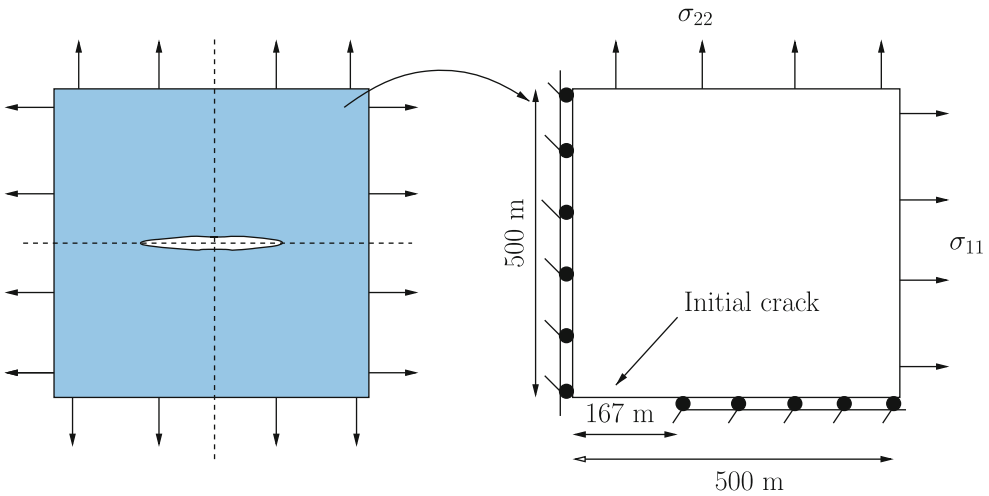

Fig. 6 Schematic representation of an ice plate with center crack loaded in biaxial tension. Only one-quarter of the domain is modeled owing to symmetry and an initial crack of length 167 m is prescribed. Stresses of $\sigma_{11} = 0.5$ MPa and $\sigma_{22} = 0.2$ MPa are applied so as to propagate the crack

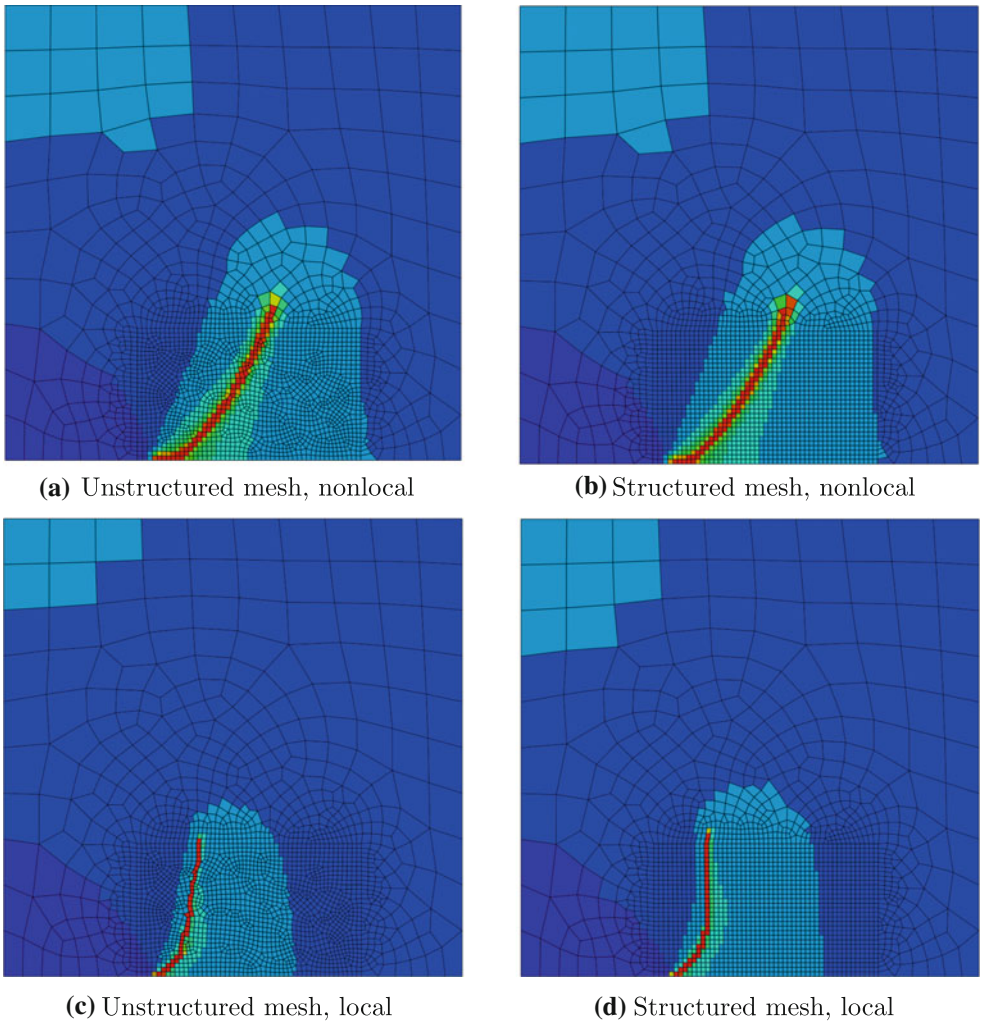

(a) Unstructured mesh, nonlocal **(b)** Structured mesh, nonlocal

(c) Unstructured mesh, local **(d)** Structured mesh, local

Fig. 7 Directional mesh bias study for the local and nonlocal damage formulations. The nonlocal damage formulation alleviate the mesh bias, therefore, is consistent

[23]. For consistency, we employ a nonlocal integral damage formulation, wherein we introduce an assumed length scale, $l_c = 10\,\text{m}$. The nonlocal scheme alleviates the issue of mesh size dependence yielding numerical results that are reasonably consistent for all meshes with $h < l_c$ (i.e., for $h = 5, 2.5, 1.25$), as shown in Fig. 5b. Also, note that the dissipation energy predicted by the nonlocal formulation for all meshes with $h < l_c$ is greater than that predicted by the local formulation, because in the nonlocal approach damage is diffused over the length scale. The simulated mode-I creep fracture pathway for $h = 1.25\,\text{m}$ is shown in Fig. 5c.

Remark 11 As noted by Bazant et al. [50], "the nonlocal averaging is unnecessary in the regions of small damage, that is, far from the fracture front. However, within the volume (or the area in 2D) of the fracture process zone some form of nonlocal averaging is necessary." Therefore, it is reasonable to assume a value of the nonlocal length scale l_c that is on the same order of magnitude as the fracture process zone. However, the relation between the characteristic length scale and a physical length scale such as the grain-size in polycrystalline materials or the aggregate-size in concrete would be much more complex.

Remark 12 In the current study we assume a value for the characteristic nonlocal length scale $l_c = 10$ m in order to improve the numerical scheme. This value l_c agrees with the estimated size of the fracture process zone of 10 m for a temperate alpine glacier in [14]. Note that the influence of size effect on the material behavior is not considered herein, although, it is possible to incorporated it into the model using the deterministic size effect law [51].

4.3 Mixed mode creep crack growth

The aim of this study is to investigate the influence of directional mesh bias of finite element computations for creep

damage. Let us consider one-quarter of a square-shaped ice plate with a crack, as shown in Fig. 6. Stresses of $\sigma_{11} = 0.5\,\text{MPa}$ and $\sigma_{22} = 0.2\,\text{MPa}$ are applied so as to propagate an inclined crack originating at the tip of the initial crack. Note that the application of biaxial tension leads to mixed-mode creep fracture propagation.

We consider two finite element meshes, one structured and the other unstructured, consisting of bilinear quadrilateral elements (CPS4 in Abaqus) with mesh size $h \approx 5\,\text{m}$. The numerical results from local and nonlocal computations are given Fig. 7. We take the anisotropy parameter $\gamma = 0$ and study the influence of mesh bias for isotropic models. Figure 7c,d clearly show that the local damage formulation suffers from directional mesh bias and its influence is more pronounced in the structured mesh results. On the other hand, the nonlocal damage formulation yields consistent results for both the structured and the unstructured meshes, as shown in Fig. 7a,b.

Remark 13 In two-dimensions, when one principal stress is positive (tension) and other principal stress is negative (compression) Murakami's anisotropic creep damage theory works well. However, under biaxial tension when both the principal stresses are positive the theory needs to be modified, wherein the anisotropy parameter γ needs to be computed at each Gauss (integration) point based on the relative magnitudes of the principal stresses [52]. Such a modification of the damage model needs further attention and will be the focus of future research. In the current work, our aim is to discuss the applicability of *nonlocal formulations for creep damage*, which has not been addressed in the literature, previously.

4.4 Creep crack propagation in glaciers

The objective of this study is to demonstrate the suitability of the proposed formulation to study crevasse propagation in glaciers. Crevasses are fractures in glaciers and ice sheets that form under tension. Herein, we use the nonlocal creep damage formulation to evaluate crevasse propagation rates in an idealized rectangular ice slab with an initial notch, as shown in Fig. 8. A constant strain rate that varies linearly with the depth is applied at the right edge of the slab so as to propagate a curved crack originating from the initial crevasse represented by the notch. The ice slab is considered to be under plane strain since the dimension perpendicular to its plane is large [53]; whereas, in the previous three examples plane stress conditions were assumed since the dimension perpendicular to its plane is small. Note that the crack propagation rate and possibly the crack orientation can be different depending on the plane stress or the plane strain assumption, which is based on the geometry of the domain.

We consider two finite element meshes, one consisting of bilinear quadrilaterals (CPE4 in Abaqus) and the other consisting of linear triangles (CPE3 in Abaqus), with mesh size $h \approx 3\,\text{m}$. The numerical results from nonlocal computations for both meshes are consistent, as shown in Fig. 9. We can see that the surface crevasses propagate through the entire depth of the glacier leading to a calving event, wherein an iceberg detaches from the glacier. The curves of crack length versus time for both the meshes are given in Fig. 10. Note that evaluating crevasse propagation rates in glacial ice can help estimate iceberg calving rates, which is important to predicting the mass loss from ice sheets and consequent sea-level rise.

5 Conclusion

To conclude, we proposed a nonlocal damage integral formulation for studying creep fracture propagation in ice. The formulation captures the tension–compression asymmetry of ice behavior and damage induced inhomogeneity and directional anisotropy, which is accomplished by calculating the material parameters at each integration point at every time step based on the current stress state. While the material parameters are specifically calibrated for ice in [17], the creep damage model is general and can be used for other creeping materials. The numerical examples presented show the suitability of the current Lagrangian finite element framework for both local and nonlocal computations. The nonlocal computations presented adequately demonstrate mesh size and mesh alignment independence, implying consistency. The numerical strategies proposed for rupture control help continue the simulations till complete structural failure. The simulations of crevasse propagation in idealized rectangular ice

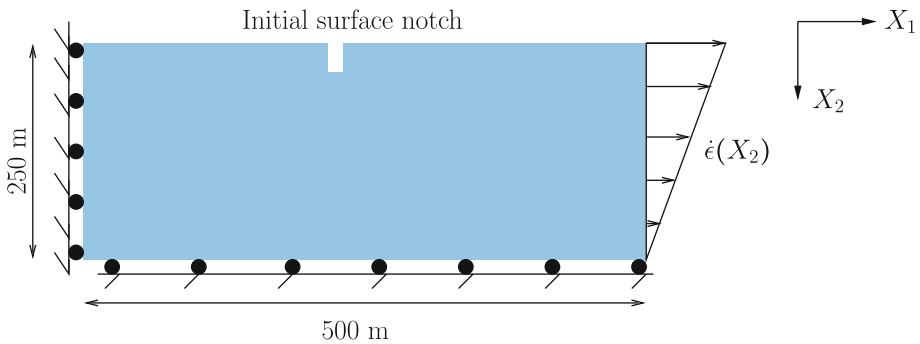

Fig. 8 Schematic representation of a notched rectangular ice slab loaded in tension. A constant strain rate that varies linearly with the depth is applied at the right edge of the slab so as to propagate a curved crack originating from the initial notch

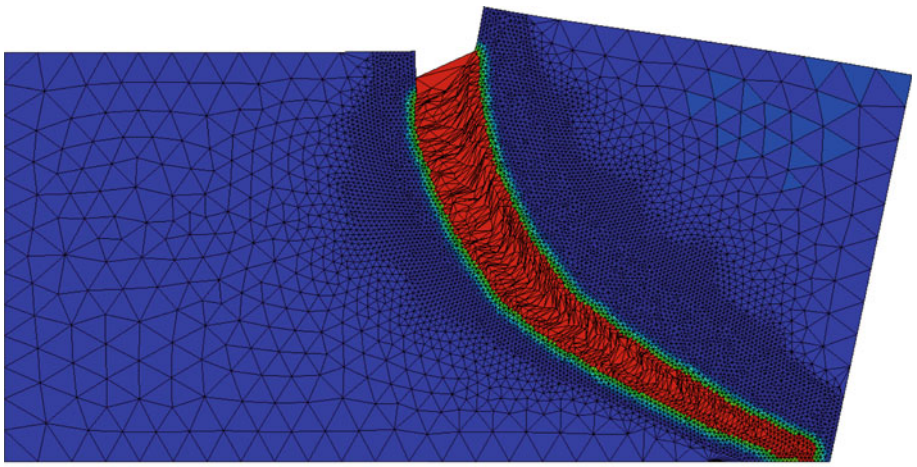

(a) Triangles (CPE3 elements in Abaqus)

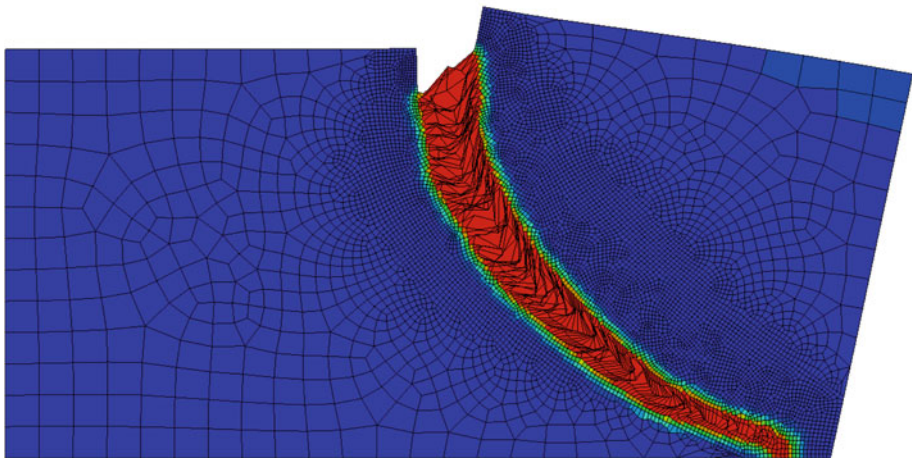

(b) Quadrilaterals (CPE4 elements in Abaqus)

Fig. 9 Creep fracture in idealized rectangular ice slabs loaded in tension. Damage contour plots are shown here and the elements colored in *red* have ruptured. The maximum damage is controlled, $D_{\max} = 0.9$, which helps continue the simulation until complete structural failure. (Please refer to the online version for plots)

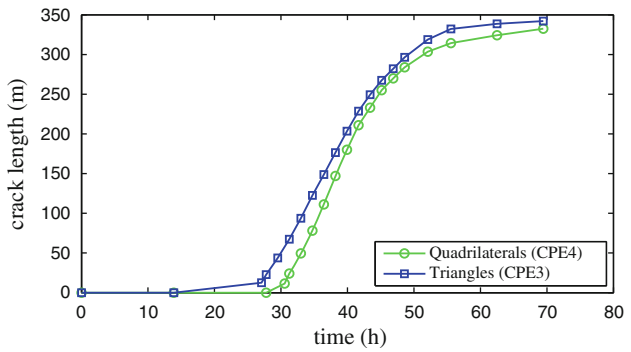

Fig. 10 Crack length versus time plots for the predicted creep fracture pathways. The applied strain rate $\dot{\epsilon}(X_2) = 0.00005 \left(\frac{X_2}{250}\right)$ m/s

slabs illustrate the applicability of the computational model to study the processes of iceberg calving and rift propagation in glaciers.

Acknowledgments The authors are grateful to the funding support provided by the Department of Energy under Grant #DE-SC0002137 (the ASCR SciDAC ISICLES initiative of DOE) and to Dr. Jeremy Bassis at University of Michigan, Ann Arbor, for the interesting discussions on iceberg calving and ice-shelf fracture.

References

1. Schulson EM, Duval P (2009) Creep and fracture of ice. Cambridge University Press, Cambridge
2. Bassis JN, Fricker HA, Coleman R, Minster J (2008) An investigation into the forces that drive ice-shelf rift propagation on the amery ice shelf, East Antarctica. J Glaciol 54(184):17–27
3. van der Veen CJ (1998) Fracture mechanics approach to penetration of surface crevasses on glaciers. Cold Reg Sci Technol 27: 31–47
4. Rist MA, Sammonds PR, Oerter H, Doake CSM (2002) Fracture of Antarctic shelf ice. J Geophys Res Solid Earth 107(B1):2002
5. Alley RB, Dupont TK, Parizek BR, Anandakrishnan S (2005) Access of surface meltwater to beds of sub-freezing glaciers: preliminary insights. Ann Glaciol 40(1):8–14
6. van der Veen CJ (2007) Fracture propagation as means of rapidly transferring surface meltwater to the base of glaciers. Geophys Res Lett 3(1):L01501
7. Nick FM, vander Veen CJ, Benn DI (2010) A physically based calving model applied to marine outlet glaciers and implications for the glacier dynamics. J Glaciol 56(199):781–794

8. Hutter K (1983) Theoretical glaciology: material science of ice and the mechanics of glaciers and ice sheets. Springer, New York
9. Mahrenholtz O, Wu Z (1992) Determination of creep damage parameters for polycrystalline ice. Paper presented at third international conference on ice technology, advances in ice technology, Massachusetts Institute of Technology, Cambridge
10. Al-Rub RKA, Voyiadjis GZ (2006) A finite strain plastic-damage model for high velocity impact using combined viscosity and gradient localization limiters: part I—theoretical formulation. Int J Damage Mech 15(4):293–334
11. Lemaitre J (1992) A course on damage mechanics. Springer, New York
12. Karr DG, Choi K (1989) A three-dimensional constitutive damage model for polycrystalline ice. Mech Mater 8(1):55–66
13. Wu Z, Mahrenholtz O (1993) Creep and creep damage of polycrystalline ice under multi-axial variable loading. Paper presented at 12th international conference on offshore mechanics and Arctic engineering, ASME, Glasgow
14. Pralong A, Funk M (2005) Dynamic damage model of crevasse opening and application to glacier calving. J Geophys Res Solid Earth 110(B1):B1309
15. Murakami S (1983) Notion of continuum damage mechanics and its application to anisotropic creep damage theory. J Eng Mater Technol Trans ASME 105(2):99–105
16. Murakami S, Kawai M, Rong H (1988) Finite-element analysis of creep crack-growth by a local approach. Int J Mech Sci 30(7): 491–502
17. Duddu R, Waisman H (2012) A temperature dependent creep damage model for polycrystalline ice. Mech Mater 46:23–41
18. Bazant ZP (1986) Mechanics of distributed cracking: review paper. Appl Mech Rev 39:665–705
19. Hall FR, Hayhurst DR (1991) Modelling of grain size effects in creep crack growth using a non-local continuum damage. Proc Math Phys Sci 433(1888):405–421
20. Zolochevsky Z, Sklepus S, Hyde TH, Becker AA, Peravali S (2009) Numerical modeling of creep and creep damage in thin plates of arbitrary shape from materials with different behavior in tension and compression under plane stress conditions. Int J Numer Methods Eng 80(11):1406–1436
21. Murakami S, Liu Y, Mizuno M (2000) Computational methods for creep fracture analysis by damage mechanics. Comput Methods Appl Mech Eng 183:15–33
22. Pijaudier-Cabot G, Bazant Z (1987) Nonlocal damage theory. J Eng Mech 113:1512–1533
23. Bazant ZP, Pijaudier-Cabot G (1988) Non-local continuum damage localisation instability and convergence. J Appl Mech 55: 287–293
24. Peerlings RHJ, DeBorst R, Brekelmans WAM, DeVree JHP (1996) Gradient-enhanced damage model for quasi-brittle materials. Int J Numer Methods Eng 39(19):391–403
25. Peerlings RHJ, Geers MGD, De Borst R, Brekelmans WAM (2001) A critical comparison of nonlocal and gradient-enhanced softening continua. Int J Solids Struct 38: 7723–7746
26. Verhoosel CV, Scott MA, Hughes TJR, de Borst R (2011) An isogeometric analysis approach to gradient damage models. Int J Numer Methods Eng 86(1):115–134
27. Al-Rub RKA, Darabi MK, Masad EA (2010) A straightforward numerical technique for finite element implementation of nonlocal gradient-dependent continuum damage mechanics theories. Int J Theor Appl Multiscale Mech 1(4):352–385
28. Hsia KJ, Argon AS, Parks DM (1991) Modeling of creep damage evolution around blunt notches and sharp cracks. Mech Mater 11(1):19–42
29. Wang XN, Wang XC (1996) Finite element analysis on creep damage. Comput Struct 60(5):781–786
30. Becker AA, Hyde TH, Sun W, Andersson P (2002) Benchmarks for finite element analysis of creep continuum damage mechanics. Comput Mater Sci 25(1-2):34–41
31. Desmorat R, Gatuingt F, Ragueneau F (2007) Nonlocal anisotropic damage model and related computational aspects for quasi-brittle materials. Eng Fract Mech 74:1539–1560
32. Jirasek M, Grassl P (2008) Evaluation of directional mesh bias in concrete fracture simulations using continuum damage models. Eng Fract Mech 75:1921–1943
33. Liu WK, Jun S, Zhang YF (1995) Reproducing kernel particle methods. Int J Numer Methods Fluids 20:1081–1106
34. Liu WK, Hao S, Belytschko T, Li S-F, Chang CT (1995) Multiple scale meshfree methods for damage fracture and localization. Comput Mater Sci 16: 197–205
35. Simo JC, Ju JW (1987) Strain-based and stress-based continuum damage models 1 formulation. Int J Solids Struct 23(7):821–840
36. Murakami S, Ohno N (1980) A continuum theory of creep and creep damage. Paper presented at 3rd symposium creep in structures, international union of theoretical and applied mechanics, Leicaster
37. Chen XF, Chow CL (1995) On damage strain energy release rate Y. Int J Damage Mech 4(1):251–263
38. Qi W, Bertram A (1999) Anisotropic continuum damage modeling for single crystals at high temperatures. Int J Plast 15(11):1197–1215
39. Lemaitre J (1971) Evaluation of dissipation and damage in metals. In: Proceedings of the international congress on the mechanical behavior of materials. I.C.M., Kyoto, p 1
40. Riedel H (1997) Fracture at high temperatures. Springer, Berlin
41. Glen JW (1955) The creep of polycrystalline ice. Proc R Soc Lond A Math Phys Sci 228(1175):519–538
42. Schulson EM (1997) The brittle failure of ice under compression. J Phys Chem B 101(32):6254–6258
43. Budd WF, Jacka TH (1989) A review of ice rheology for ice-sheet modeling. Cold Reg Sci Technol 16(2):107–144
44. Voyiadjis GZ, Al-Rub RKA, Palazotto AN (2004) Thermodynamic framework for coupling of non-local viscoplasticity and non-local anisotropic viscodamage for dynamic localization problems using gradient theory. Int J Plast 20(6):981–1038
45. de Borst R, Sluys LJ, Mühlhaus H-B, Pamin J (1993) Fundamental issues in finite element analysis of localization of deformation. Eng Comput 10:99–121
46. Hibbitt, Karlsson, Sorensen, Inc. (2011) Abaqus/standard user's manual v. 6.9. Pawtucket, Rhode Island
47. Chow CL, Mao J, Shen J (2011) Nonlocal damage gradient model for fracture characterization of aluminum alloy. Int J Damage Mech 20(7):1073–1093
48. Jirasek M, Patzák B (2002) Consistent tangent stiffness for non-local damage models. Comput Struct 80(14–15):1279–1293
49. Krausz AS (1963) The creep of ice in bending. Can J Phys 41(1):167–177
50. Bazant Z, Xi Y, Reid S (1991) Statistical size effect in quasi-brittle structures: II nonlocal theory. J Eng Mech 117(11):2623–2640
51. Bazant ZP (1999) Size effect on structural strength: a review. Arch Appl Mech 69(9–10):703–725
52. Ganczarski A, Skrzypek J (2001) Application of the modified Murakami's anisotropic creep damage model to 3D rotationally-symmetric problem. Tech Mech 21(4):251–260
53. Weertman J (1957) On the sliding of glaciers. J Glaciol 3(21): 33–38